Applied Catalysis B: Environmental 148–149 (2014) 357–365

Contents lists available at ScienceDirect

Applied Catalysis B: Environmental

journal homepage: www.elsevier.com/locate/apcatb

Carbon nanofibres coated with Ni decorated MoS_2 nanosheets as catalyst for vacuum residue hydroprocessing

J.L. Pinilla[a], H. Purón[a], D. Torres[b], S. de Llobet[b], R. Moliner[b], I. Suelves[b,*], M. Millan[a,**]

[a] Department of Chemical Engineering, Imperial College London, London SW7 2AZ, UK
[b] Instituto de Carboquímica (CSIC), Miguel Luesma 4, Zaragoza 50018, Spain

ARTICLE INFO

Article history:
Received 5 August 2013
Received in revised form
12 November 2013
Accepted 13 November 2013
Available online 21 November 2013

Keywords:
Carbon nanofibers
MoS_2
Vacuum residue
Hydroprocessing

ABSTRACT

Catalysts based on functionalised carbon nanofibers (FCNF) coated with Ni-decorated MoS_2 nanosheets were obtained by direct decomposition of ammonium thiomolybdate and nickel nitrate impregnated on the FCNF under controlled temperature conditions in inert atmosphere. The catalysts were characterised by X-ray diffraction (XRD), N_2 adsorption, Raman spectroscopy, temperature programmed reduction of sulfur species (TPR-S), NH_3 temperature programmed desorption (NH_3-TPD) and transmission electron microscopy (TEM). Decomposition temperature was found to have a paramount importance in the formation of uniform MoS_2 slabs, as revealed by the TEM study: at 600 °C, non-uniform covering of the carbon nanofiber (CNF) was observed together with the presence of small round-shaped metal particles (ca. 20 nm). On the other hand, at 450 °C CNF appeared homogeneously covered by amorphous MoS_2 slabs decorated with Ni, resulting in higher amount of coordinated unsaturated sites (CUS), as determined by TPR-S. Catalysts were tested in the hydroprocessing of a vacuum residue and the results were compared against a benchmark alumina-supported NiMo catalyst. Higher asphaltene conversions were obtained for the CNF-supported catalysts prepared at 450 °C, which overperformed the Al_2O_3-supported benchmark catalyst. However, the catalytic performance in hydrodesulfurisation and hydrodemetallisation of the CNF-based catalysts was slightly lower than that of the benchmark catalyst.

1. Introduction

Carbon materials have been extensively studied as catalytic support due to their outstanding textural properties and tunable chemical nature [1,2]. The discovery of carbon nanotubes (CNT) by Iijima [3] increased the interest in carbon nanofilaments, including CNT and carbon nanofibers (CNF). These structures of ca. 10–100 nm in diameter and several micrometres in length are formed by graphitic planes (graphenes) disposed with different arrangements. CNT and CNF are typically produced by the decomposition of various fossil hydrocarbons [4] or renewable sources such as biogas [5,6] on catalysts based on transition metals (Ni, Fe and Co) supported on different metal oxides [4]. Different chemical structures of CNT (single wall and multi wall) and CNF (platelet, fishbone and ribbon) can be obtained [7,8]. The carbon nanofilament morphology depends on variables such as the metal used in the catalyst, metal crystal size, carbon gas source and synthesis conditions [4].

Carbon nanofilament aggregates are characterised by having extremely open morphology with minimal or no microporosity, relatively large pore volumes generated by the empty space between the tubular structures, as well as significantly high surface area, mainly derived from the external wall surface area of the nanofilaments. These characteristics make them promising catalyst supports for liquid phase reactions, since mass transfer limitations are prevented due to the availability of the active sites on the outer section of the carbon nanofilaments [9]. In addition, some studies indicated higher hydrodesulfurisation (HDS), hydrodenitrogenation (HDN) and hydrodemetallisation (HDM) activity of carbon-supported catalysts compared to those supported on Al_2O_3, as reviewed in [10]. This higher activity was attributed to a more efficient activation of metal sites and transfer of hydrogen to reactant molecules [11,12]. Additionally, the lower metal–support interaction compared to typical acid supports such as alumina and zeolites makes a larger fraction of active phase available to the reactants. This fact allows an easier and deeper metal oxide reduction and sulfidation [13–15].

Catalysts supported on CNF have been used in fuel cell applications [16], chemical synthesis such as hydrogenation [17], higher alcohol synthesis [18] and Fischer–Tropsch reactions [19]. Some examples that show the potential of these materials in hydroprocessing reactions of both model compounds and real feeds can

* Corresponding author. Tel.: +34 976733977; fax: +34 976733318.
** Corresponding author. Tel.: +44 2075941633; fax: +44 2075945638.
E-mail addresses: isuelves@icb.csic.es (I. Suelves), marcos.millan@imperial.ac.uk (M. Millan).

0926-3373/$ – see front matter © 2013 Elsevier B.V. All rights reserved.
http://dx.doi.org/10.1016/j.apcatb.2013.11.019

be found in the literature. Multi-walled CNT (MWCNT) supported catalysts were studied in the HDS of thiophene [14] and dibenzothiophene [20] and in the HDN of pyrrole [14]. Fishbone and platelet CNF were studied in the HDS of thiophene [15]. However, studies with real feeds using catalysts supported on nanostructured carbon (NC) are scarce. CNT impregnated with Co and Mo were used as catalysts for vacuum residue (VR) hydrocracking [21]. NiMo supported on acid-treated MWCNT were tested with a light gas oil (LGO) derived from Athabasca bitumen [13]. It was observed that CNT or CNF-supported catalysts yielded significantly less amount of coke than an Al_2O_3-supported catalyst under the same reaction conditions. This is commonly attributed to the lower acidity of the carbon-nanofilament-based catalysts. However, their performance may also depend upon factors such as the feed and type of reactor used. To the best of our knowledge, asphaltene upgrading and HDM activity using CNF- or CNT-based catalysts towards real feeds have not been addressed in the literature.

In this work, fishbone CNF were coated with MoS_2 nanosheets decorated with Ni. This was achieved by thermally decomposing the CNF impregnated with ammonium thiomolybdate (ATM) and nickel nitrate in an inert atmosphere. The effect of the decomposition temperature on the uniformity and homogeneity of the MoS_2 slabs was evaluated. These catalysts were characterised by a number of techniques such as N_2 adsorption, X-ray diffraction, Raman spectroscopy, temperature programmed reduction of sulfur species and transmission electron microscopy. Catalyst performance in heavy oil hydroprocessing was investigated using a real oil-derived feed, a vacuum residue from a Maya oil. Results in terms of liquid product upgrading (asphaltenes and fraction with boiling point above 450 °C), HDM (nickel and vanadium) and HDS conversions are presented and compared against a benchmark NiMo/Al_2O_3 catalyst.

2. Experimental

2.1. Catalyst support synthesis

2.1.1. CNF synthesis and functionalisation

Fishbone-like CNFs were produced at large scale in a rotary bed reactor described elsewhere [22] using a Ni/Al_2O_3 catalyst. The as-prepared CNF will be referred to as CNF in this work. Hydrocarbon feedstock was composed by a mixture of CH_4:CO_2 (1:1). Synthesis conditions used were 700 °C and a weight hourly space velocity of 30 L·(g_{cat} h)$^{-1}$. More details about the catalyst properties and process conditions can be found elsewhere [6]. CNF functionalisation was performed by reflux in concentrated HNO_3 (Panreac, 65%) during 30 min. Finally, functionalised CNF (FCNF) were filtered, washed with distilled water until the pH was above 6 and dried at 100 °C overnight.

2.1.2. Mesoporous alumina synthesis

An alumina support with large surface area and pore volume was synthesised according to a procedure [23] modified from the literature [24].

2.2. Catalyst synthesis

Carbon-based catalysts were prepared by the incipient wetness impregnation method. Successive impregnations of the precursor salts, $(NH_4)_2MoS_4$ and $Ni(NO_3)_2$ were performed with intermediate drying steps at 80 °C for 12 h. The dilution calculations were based on the wettability of the supports for the following concentrations: 9.3 wt% Mo and 2.4 wt% Ni. After impregnation, catalysts were tempered either at 450 or 600 °C in a tubular reactor electrically heated under flowing N_2 at 50 mL min^{-1} for 4 h, in order to allow the decomposition of the metal precursors and simultaneously avoid the oxidation of the CNF that would take place during the typical calcination step in air. Catalysts are denoted as NiMo/FCNF-T hereafter, where T refers to the decomposition temperature.

The alumina-supported catalyst used as a benchmark was prepared following the same procedure described for the carbon-based catalysts. The metal loading for this catalyst was the same as for the carbon-supported ones. After impregnation, the catalyst was calcined in a muffle furnace at 500 °C for 4 h under air flowing at 200 mL min^{-1}. This catalyst is denoted as NiMo/Al_2O_3.

2.3. Characterisation techniques

The textural properties of the carbonaceous support and NiMo catalysts were measured by N_2 adsorption at −196 °C in a Micromeritics Tristar apparatus. The specific surface areas and pore volumes were calculated by applying the BET method to the respective N_2 adsorption isotherms and the pore size distribution was calculated by the BHJ method based on the desorption branch of the isotherm.

The determination of the amount of surface oxygen created during the functionalisation treatments was carried out by temperature programmed desorption (TPD) in an AutoChem II 2920 apparatus. The profiles of released CO and CO_2 were obtained in a quartz reactor heated under a constant flow of Ar (50 mL min^{-1}) at a heating rate of 10 °C min^{-1}, up to a temperature of 1000 °C. The eluted gas was analysed by mass spectroscopy. The total amount of CO and CO_2 released was calculated by integrating the area under of the concentration curve versus volume.

The remaining content of the Ni/Al_2O_3 used to grow the CNF was analysed in the CNF and FCNF by temperature programmed oxidation (TPO). This was obtained in a Setaram Thermogravimetric Analyzer by heating the sample under air flow at a rate of 10 °C min^{-1}. Ni oxidation was taken into account to calculate the catalyst content in the as-prepared carbon nanofibers.

Powder X-ray diffraction patterns of fresh and tempered catalysts were acquired in a PANalytical diffractometer equipped with a Ni-filtered Cu $K\alpha$ radiation and a secondary graphite monochromator, using a θ–2θ configuration.

Raman spectra of the carbonaceous materials were obtained with a Horiba Jobin Yvon HR800 UV microspectrometre using the green line of an argon laser (λ = 532 nm) as the excitation source.

Temperature programmed reduction of sulfided samples (TPR-S) was performed in a PulseChemisorb 2700 apparatus equipped with a thermal conductivity detector (TCD). The amount of sample used was approximately 200 mg. Temperature was increased from room temperature to 600 °C at a rate of 10 °C min^{-1} under a flow rate of 50 mL min^{-1} of a H_2 (10%)/Ar mixture.

NH_3-temperature programmed desorption of the fresh catalysts was carried out in the same apparatus used for the TPR-S analysis. The catalyst (200 mg) was outgassed in argon flow, heated to 600 °C at a rate of 10 °C min^{-1}, and kept at 600 °C for 1 h. The sample was cooled down to 50 °C and allowed to adsorb ammonia. After purging the physically adsorbed ammonia, the system was heated to 600 °C under Ar flow. The amount of chemisorbed ammonia was detected with a TCD.

Transmission Electron Microscopy was carried out on a Jeol 2011 microscope equipped with a LaB_6 gun and operating at 200 kV. The samples were first finely grounded, dispersed in ethanol and a drop of solution was then deposited on a standard TEM copper grid, previously covered by a lacey amorphous carbon film.

Carbonaceous deposits on the spent catalysts were determined with a Pyris TGA1 thermogravimetric analyser. Samples of approximately 3 mg were combusted from 50 to 900 °C at a rate of 10 °C min^{-1} with an air flow of 40 mL min^{-1}. The samples were held at isothermal conditions for the initial and final temperatures to allow the weight to stabilise. Coke deposits were determined as

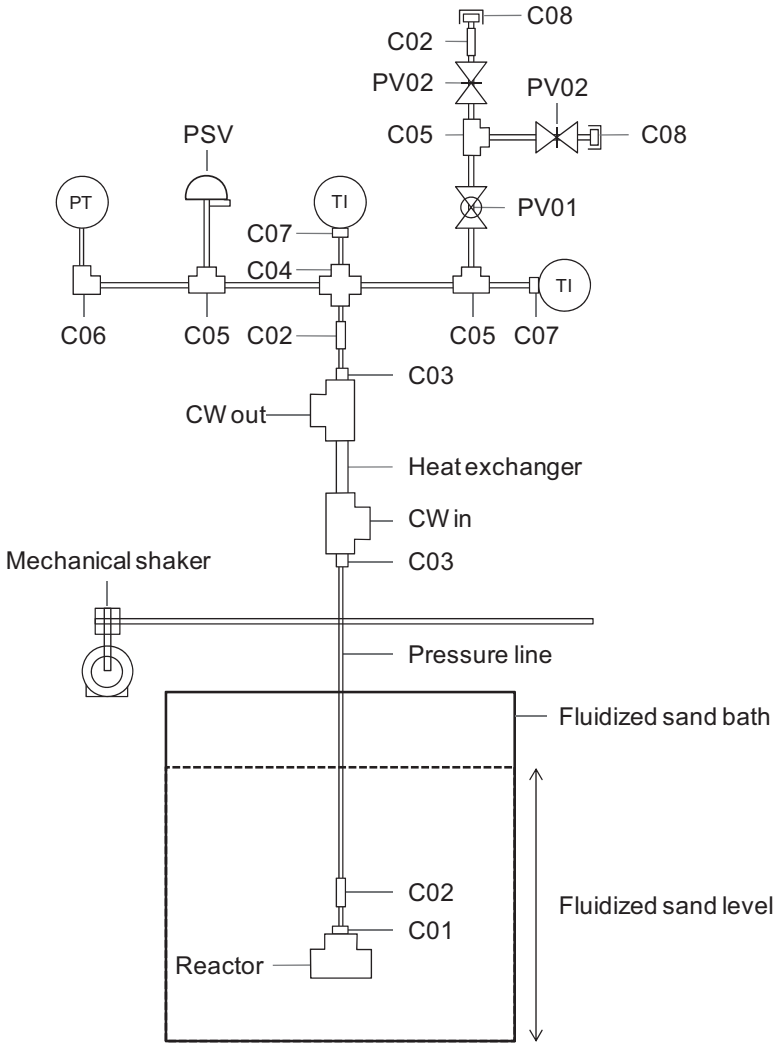

Fig. 1. Microbomb reactor diagram. Where: PT—pressure transducer, TI—temperature indicator, PSV—relief valve, PV01—ball valve, PV02—needle valve, C01—1/2 in. to 1/4 in. reducing port connector, C02—1/4 in. straight union, C03—1/4 in. to 1/2 in. reducer, C04—1/4 in. union cross, C05—1/4 in. union tee, C06—1/4 in. union elbow, C07—1/4 in. to thermocouple reducer, C08—1/4 in. cap.

the difference in weight loss between the fresh and spent carbon-supported catalysts in the region where coke deposits occurred (300–500 °C). The carbonaceous deposits on the $NiMo/Al_2O_3$ catalyst were calculated as the difference between the initial stabilised weight and the final stabilised weight. In both cases, oxidation of MoS_2 and NiS_2 species was taken into account to calculate the coke content on the spent catalysts.

2.4. Vacuum residue hydroprocessing tests

A batch microbomb reactor described elsewhere [25] was used for the hydroprocessing reactions. A diagram of the reactor is shown in Fig. 1. Briefly, the reactor consisted in a 1/2 in. bored-through Swagelok union tee with both ends plugged and connected to a pressurising line. During operation the reactor was placed inside a heated fluidised sand bath and connected to a reactor shaker assembly for stirring. The feed consisted in 0.5 g of a vacuum residue (VR), which was used in a 4:1 wt/wt ratio with the catalyst. 0.1 mL of CS_2 was added in order to keep the catalysts in the sulfided state during the runs. Reactions were carried out at 15 MPa of H_2 cold pressure and 425 °C with contact time of 1 h, defined as the holding time at the desired reaction temperature. At the end of the run, the reactor was first quickly quenched with cold water to ambient temperature to stop reactions and then depressurised.

Samples were carefully recovered from the reactor with a solvent mixture of $CHCl_3/CH_3OH$ 4:1 vol/vol and the catalysts were separated from the products by filtration. The liquid products were dried to constant weight. The solids were washed with solvent to ensure all soluble materials were removed and they were afterwards dried in vacuum at 60 °C for 3 h.

2.5. VR and product characterisation techniques

The VR sample utilised was obtained from Maya crude oil, a heavy oil with a large heteroatom content. The main physicochemical properties of the VR are described in Table 1. VR presents high asphaltene, sulfur and metal contents. It is solid at ambient conditions and was used as received without dilution.

Liquid products were recovered after each reaction and fractioned into maltenes (heptane soluble) and asphaltenes (heptane insoluble, toluene soluble) following a procedure previously described [23]. Afterwards, the maltene fraction was analyzed by gas chromatography (GC). A Perkin Elmer Clarus 500 Chromatographer fitted with a flame ionisation detector (FID) was used to quantify the boiling point distribution below 450 °C in the maltene

Table 1
VR properties.

Boiling point interval (°C)	450+
Specific gravity at 15 °C	1.08
°API gravity	−0.34
Viscosity at 100 °C (cSt)	265,546
Sulfur content (wt%)	7.02
Conradson carbon (wt%)	25.54
Asphaltenes (wt%)	33.63[a]
Ni (ppm w/w)	93[a]
V (ppm w/w)	227[a]

[a] Determined with the same method as reaction products.

fraction. The GC was equipped with a SGE capillary column (HT-5, 25 m long, 0.1 μm film thickness) and was operated in split mode (split ratio 1:20) with helium as a carrier gas using the ASTM 2887 method. A calibration using Standard Gas Oil (Sigma Aldrich) was performed to evaluate the percentage of elution of the material.

The conversion of materials boiling above 450 °C, $C_{>450\,^\circ C}$, and the conversion of the asphaltene fraction, $C_{\text{Asphaltenes}}$, were calculated with Eqs. (1) and (2), respectively. These conversion definitions take into account carbonaceous deposits on the catalysts as unconverted feed. This allows for a distinction between active catalysts and catalysts that merely lead to large carbon deposits [26].

$$C_{>450\ ^\circ C} = \frac{m_F \times x^F_{>450\ ^\circ C} - m_{LP} \times x^{LP}_{>450\ ^\circ C} - m_{SP} \times x^{SP}_{\text{carbon}}}{m_F \times x^F_{>450\ ^\circ C}} \quad (1)$$

$$C_{\text{Asphaltenes}} = \frac{m_F \times x^F_{\text{Asphaltenes}} - m_{LP} \times x^{LP}_{\text{Asphaltenes}} - m_{SP} \times x^{SP}_{\text{carbon}}}{m_F \times x^F_{\text{Asphaltenes}}} \quad (2)$$

where m_F, m_{LP}, and m_{SP} are the weight of the feed, liquid products and solid products, respectively; $x^F_{>450\ ^\circ C}$ and $x^{LP}_{>450\ ^\circ C}$ are the mass fraction boiling above 450 °C in the feed (with a value of 1.0) and liquid products, correspondingly. $x^{LP}_{>450\ ^\circ C}$ was calculated by adding the maltene fraction that did not elute in GC measurements, i.e. with a boiling point above 450 °C, to the asphaltene fraction of the sample. x^{SP}_{carbon} is the amount of carbonaceous material deposited on the catalyst determined by TGA measurements in grams of carbon per gram of catalyst units. $x^F_{\text{Asphaltenes}}$ and $x^{LP}_{\text{Asphaltenes}}$ are the asphaltene mass fractions in the feed and liquid products, respectively.

Gas yield was calculated by difference according to Eq. (3).

$$\text{Gas yield} = \frac{m_F - m_{LP} - m_{SP} \times x^{SP}_{\text{carbon}}}{m_F} \quad (3)$$

Product samples were analysed with energy dispersive XRF to determine sulfur content. Measurements were performed using a Bruker S4 Pioneer with a Cu source. The sulfur content was used to calculate the HDS conversion through Eq. (4).

$$\text{Sulfur conversion, HDS} = \frac{m_F \times x^F_S - m_{LP} \times x^{LP}_S}{m_F \times x^F_S} \quad (4)$$

where x^F_S and x^{LP}_S are the mass fraction of S in the feed and liquid products, respectively.

The determination of Ni and V content in the VR and reaction products was performed with a Perkin Elmer inductively coupled plasma optical emission spectrometer (Optima 2000 DV). The analytical emission lines for Ni and V were 231.6 and 292.5 nm, respectively. This technique was utilised to determine the hydrodemetallisation activity of the catalyst. Ni and V

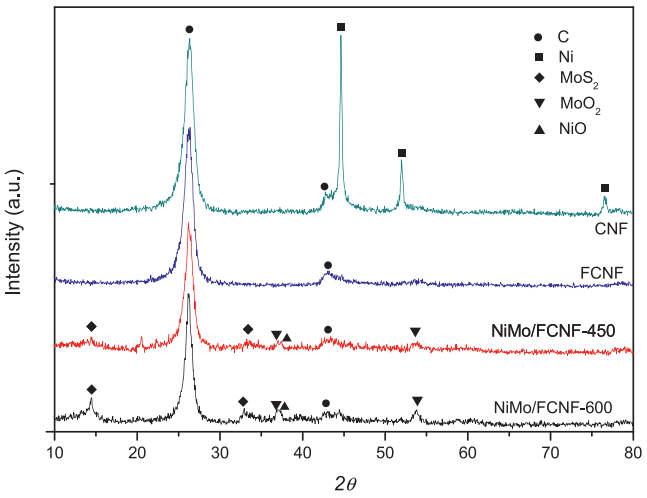

Fig. 2. Powder XRD patterns of CN, FCNF and NiMo catalysts supported on FCNF after decomposition at 450 and 600 °C.

conversions were calculated using Eqs. (5) and (6), respectively. HDM conversion was calculated from Eq. (7).

$$\text{Ni conversion, } C_{\text{Ni}} = \frac{m_F \times x^F_{\text{Ni}} - m_{LP} \times x^{LP}_{\text{Ni}}}{m_F \times x^F_{\text{Ni}}} \quad (5)$$

$$\text{V conversion, } C_{\text{V}} = \frac{m_F \times x^F_{\text{V}} - m_{LP} \times x^{LP}_{\text{V}}}{m_F \times x^F_{\text{V}}} \quad (6)$$

$$\text{HDM conversion} = \frac{m_F \times \left(x^F_{\text{Ni}} + x^F_{\text{V}}\right) - m_{LP} \times \left(x^{LP}_{\text{Ni}} + x^{LP}_{\text{V}}\right)}{m_F \times \left(x^F_{\text{Ni}} + x^F_{\text{V}}\right)} \quad (7)$$

where x^F_{Ni}, x^{LP}_{Ni}, x^F_{V} and x^{LP}_{V} are the mass fraction of Ni and V in the feed (F) and liquid products (LP), respectively.

3. Results and discussion

3.1. Support characterisation

In order to employ CNF as catalyst supports, their surface properties need to be modified to remove catalyst particles remaining from the CNF production step and to create the necessary functionalities (oxygen surface groups) that allow the active metal particles to be anchored onto the support with good dispersion. Different treatments have been developed [27]. Acid treatments enhance the surface wettability by polar solvents, thus enabling a better contact between the support and the metallic precursor solution during the impregnation step [2]. To this end, the CNF were subjected to HNO_3 acid treatment. A comparative study of the textural, surface and morphological characteristics of CNF and FCNF is presented in this section.

Fig. 2 shows the XRD pattern of the CNF, functionalised CNF, and FCNF-supported catalysts. All materials showed a prominent reflexion at ca. 26° and a weak peak at ca. 43° assigned to graphitic carbon (planes 0 0 2 and 1 0 0, respectively). The CNF revealed the presence of metallic nickel (reflexions at 44.6°, 52° and 76.6°), the active phase in the Ni/Al_2O_3 catalyst used to grow the carbonaceous structures. No significative changes in reflexions assigned to C were observed after the functionalisation treatment used. Conversely, Ni reflexions disappeared after the functionalisation treatments, revealing the effectiveness of the method employed for the removal of the metal particles originally present in the CNF structure. This fact was further confirmed using TPO experiments, presented in Table 2, which revealed that the amount of catalyst (Ni/Al_2O_3)

Table 2
Surface chemistry measured by TPD and metal content determined by TPO in as prepared CNF and FCNF. Textural properties determined by N_2 adsorption, and acidity calculated from NH_3-TPD of as prepared CNF, FCNF and supported catalysts (NiMo/FCNF-450NiMo/FCNF-600). Data of a benchmark catalyst ($NiMo/Al_2O_3$) are also included for comparison purposes.

Sample	Metal content (%)	S_{BET} ($m^2\,g^{-1}$)	V_p ($cm^3\,g^{-1}$)	APD* (nm)	Acidity ($\mu mol\,NH_3\,g^{-1}$)	CO ($mmol\,g^{-1}$)	CO_2 ($mmol\,g^{-1}$)
CNF	11.2	87.7	0.24	14.3	414.1	0.331	0.079
FCNF	1.6	98.8	0.26	14.4	1146.9	0.796	0.336
NiMo/FCNF-450	–	65.2	0.20	15.6	77.2	–	–
NiMo/FCNF-600	–	73.8	0.20	14.4	66.1	–	–
$NiMo/Al_2O_3$	–	342.5	0.56	10.4	1574	–	–

* BJH model applied to the adsorption branch of the isotherms.

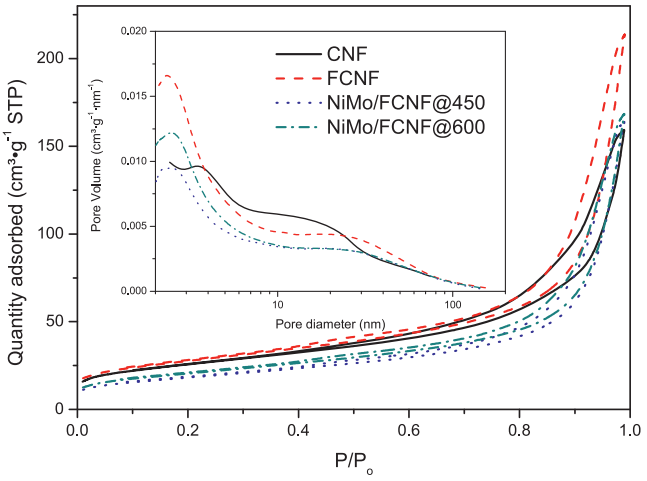

Fig. 3. N_2 adsorption–desorption isotherms and pore size distribution curves (inset) for CN, FCNF and NiMo catalysts supported on FCNF after decomposition at 450 and 600 °C.

originally in the CNF (11.2%) was significantly reduced after the oxidation treatment down to values of 1.6%. Besides, TPD experiments showed a large number of oxygen surface groups created after the functionalisation treatment, as inferred from the desorption of CO_2 and CO shown in Table 2. Acidic groups are known to decompose into CO_2, assigned mainly to carboxylic acids, carboxylic anhydrides and lactones surface groups. Basic and neutral groups are decomposed into CO, corresponding to phenols, ethers, quinines and carbonyls oxygen surface groups [28]. A three-fold increase in total acidity after the functionalisation treatment was determined by NH_3-TPD (Table 2).

The CNF presented a Type IV N_2 adsorption–desorption isotherm (Fig. 3) typically assigned to mesoporous materials with hysteresis loop H3, corresponding to condensation taking place in mesopores and plate-like particles in parallel with slit-shaped pores [29]. The shape of the isotherm did not change after the functionalisation treatment, although a slight increment in surface area was observed (Table 2). The CNF showed a specific surface area (S_{BET}) of 88 $m^2\,g^{-1}$ and a pore volume of 0.24 $cm^3\,g^{-1}$. The functionalisation treatment carried out with HNO_3 caused a slight increment in both S_{BET} and pore volume (ca. 10%). The removal of the metal particles from the tip of the carbon filaments can account for the slight increment in surface area of the FCNF observed in Table 2. However, the average pore diameter was not affected by the functionalisation treatment. Pore size distribution curves are shown in the inset of Fig. 3.

In order to reveal the effect of the functionalisation treatment on the morphology of the CNF, a TEM study was carried out. Fig. 4 shows some representative micrographs of the CNF (Fig. 4a–c). A low magnification micrograph (Fig. 4a) shows the presence of long filaments emerging from the metal particles. CNF growth mechanism is known to occur upon a series of different stages involving: hydrocarbon decomposition on the leading face of the catalyst particle, carbon production and migration to the opposite side of the catalyst particle, and further precipitation in form of tubular structures [30–32]. Higher magnification (Fig. 4b) revealed the typical diamond-shaped particle located at the tip of the growing filaments. The morphology of the nickel particle is of paramount importance in determining the growth type of the tubular structures [4]. Thus, fishbone-like CNF, which are characterised by an arrangement of the graphene planes with a certain inclination with respect to the fibre axis, are obtained. This is clearly shown in Fig. 4c, as a result of the diamond-shaped nickel particle. FCNF appear more disentangled compared to CNF, as the low magnification pictures of FCNF revealed (Fig. 4d). The HNO_3 functionalisation treatment removed the metal particles from the tip of the CNF (Fig. 4e), although it did not modify the morphology of the CNF and the fishbone-like arrangement of the graphitic planes, as shown in Fig. 4f.

3.2. NiMo supported catalysts characterisation

FCNF was sequentially impregnated with solutions containing ATM and $Ni(NO_3)_2$. After impregnation and drying of the precursor salts, a step at two different temperatures (450 and 600 °C) under N_2 flow was carried out in order to decompose the salts and obtain the metal active phase, i.e. MoS_2 decorated with Ni.

Fig. 5 shows some representative TEM micrographs of the NiMo/FCNF-450 ((a)–(c)) and NiMo/FCNF-600 ((d) and (e)) catalysts. In both samples, carbon nanofilaments were partially covered by long nanosheets with different stacking degrees. Distinct features were observed as a function of the treatment temperature. Carbon filaments in NiMo/FCNF-450 were homogeneously covered by long slabs, as observed in Fig. 5a. Higher magnification TEM micrographs (Fig. 5b and c) revealed slab-like structures coating the FCNF with a stacking degree ranging from 2 to 5. On the other hand, NiMo/FCNF-600 had a less homogenous covering of the FCNF, where some coated nanofilaments coexisted with uncovered FCNF, as shown in Fig. 5d. The presence of small round-shaped metal particles (ca. 20 nm) inserted into the tubular structures was also observed (Fig. 5e). These metal particles were not observed in sample NiMo/FCNF-450. A detail of a partially covered FCNF can be seen in Fig. 5f, with a stacking degree of ca. 2–3 slabs. In both samples, the interlayer spacing between the slabs that coated the FCNF was 0.61 nm, similar to the *d*-spacing observed in MoS_2-coated MWCNT [33,34], and higher than the typical interlayer spacing observed for the graphitic planes that formed the FCNF (0.34 nm) (Fig. 4c).

The chemical nature of the coating layers was further confirmed by XRD and Raman, revealing the formation of MoS_2. XRD diffractograms of the NiMo/FCNF catalysts (Fig. 2) showed the presence of reflections assigned to graphitic carbon, as observed for CNF and FCNF. However, the appearance of a diffraction peak at 2θ: 14.1°, characteristic of the (0 0 2) basal plane of crystalline MoS_2, was also observed. The intensity of this peak was higher in the sample tempered at 600 °C. ATM is known to decompose under inert atmosphere into MoS_3 at 260 °C and into amorphous MoS_2

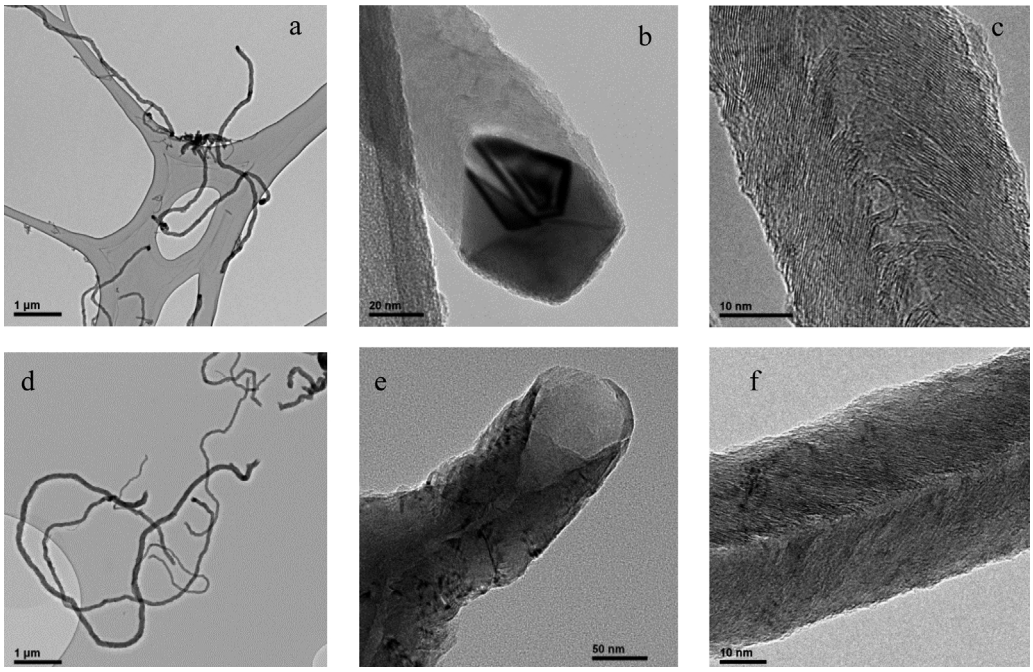

Fig. 4. Representative TEM micrographs at different magnifications of as produced CNF ((a)–(c)) and FCNF ((d)–(f)).

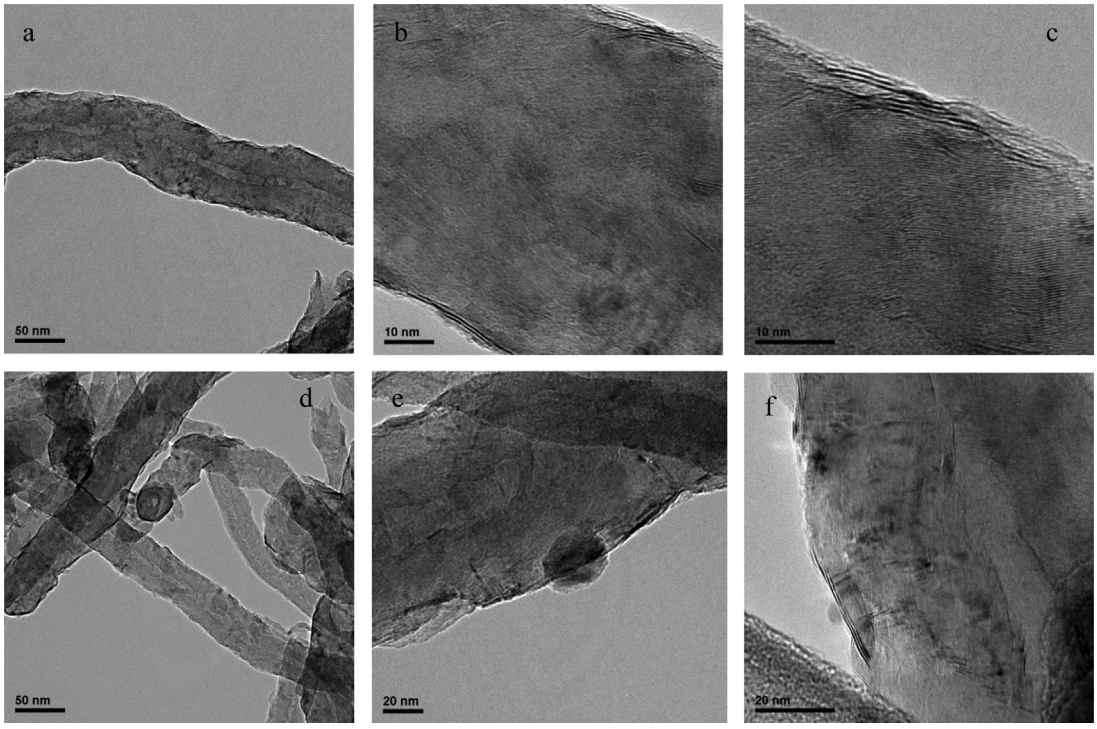

Fig. 5. Representative TEM micrographs at different magnifications of FCNF supported catalysts: NiMo/FCNF-450 ((a)–(c)); NiMo/FCNF-600 ((d)–(e)).

at higher temperatures (300–500 °C) [35]. The formation of crystalline MoS_2 by a re-stacking of the sulfide at temperatures above 500 °C has been reported [36], thus explaining the formation of larger crystallites for NiMo/FCNF-600. This sample also shows MoS_2 diffraction peaks at 33.1°, which correspond to the (1 0 0) plane. Additionally, weak reflections that can be assigned to MoO_2 and NiO were observed in the NiMo/FCNF-600 diffractogram. No evidence of nickel sulfide crystalline phases was observed by XRD.

Representative Raman spectra of the FCNF and FCNF-supported catalysts are presented in Fig. 6. All samples showed two well-resolved bands: the D band (at ~1340 nm), related to graphite imperfections, and the G band (at ~1570 nm), associated with the in-plane carbon–carbon stretching vibrations of graphite layers. The D′ band also appears close to the main graphitic band (~1600 cm^{-1}). The intensity ratio I_D/I_G did not vary to a great extent between the FCNF and FCNF-supported catalysts (results not shown). In the Raman spectrum of NiMo/FCNF-600 two new bands, occurring at ca. 380 and 405 cm^{-1}, were observed, which are assigned to the $E_{2g}{}^1$ and A_{1g} vibrational modes of crystalline MoS_2, respectively [37]. Some low intensity bands

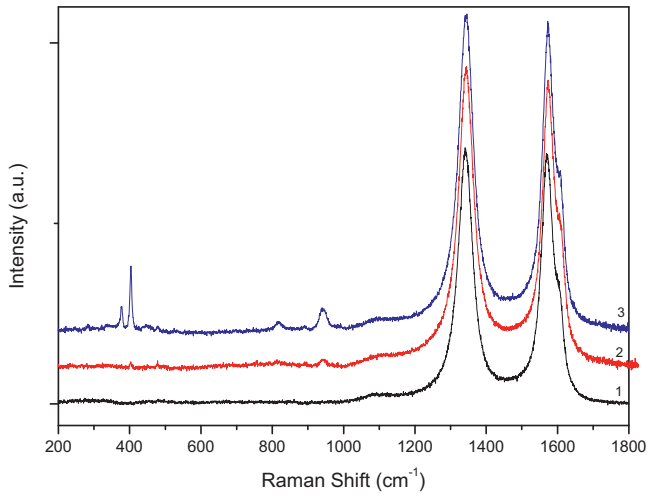

Fig. 6. Raman spectra of (1) FCNF (2) NiMo/FCNF-450 and (3) NiMo/FCNF-600.

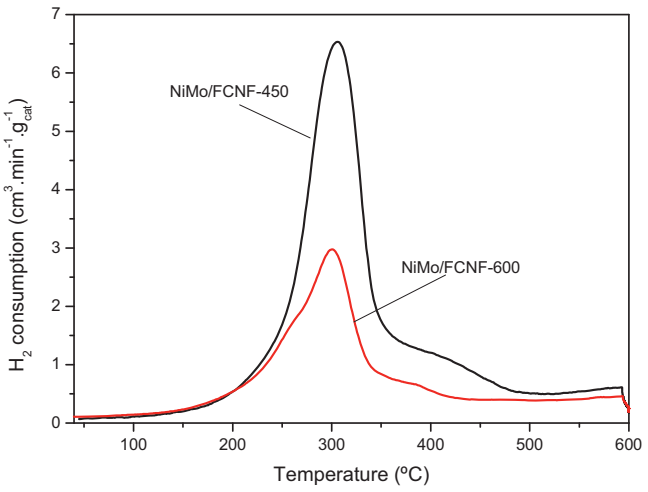

Fig. 7. TPR-S of NiMo/FCNF-450 and NiMo/FCNF-600.

in the molybdenum–oxygen stretching fundamental region (800–1000 cm^{-1}) [38] appeared, which can be tentatively assigned to oxidation of MoS_2 by exposure to ambient oxygen and possibly also by the heat generated in-situ by the laser [39]. The bands assigned to MoS_2 and MoO_3 were also present in the NiMo/FCNF-450 sample, although the intensity of these signals was much lower in comparison with those in NiMo/FCNF-600.

Fig. 3 shows the N_2 isotherm of the catalysts, which indicated that the mesoporous nature of the FCNF was maintained after metal impregnation and further decomposition of the materials, independently of the decomposition temperature used. In both cases, isotherms of Type IV with hysteresis loop H3 were observed, as for CNF and FCNF. However, impregnation of the supports resulted in a reduction in specific surface area and pore volume, as shown in Table 2. S_{BET} of NiMo/FCNF-450 and NiMo/FCNF-600 were 65.2 and 73.8 $m^2\,g^{-1}$, respectively, representing a reduction of ca. 30% in comparison with the original FCNF. The average pore diameter of NiMo/FCNF-600 did not change after impregnation of the metals while the average pore diameter of NiMo/FCNF-450 showed a slight increase. The pore size distribution shown in the inset of Fig. 3 revealed that the variation in the textural parameters in FCNF-supported catalysts was mainly due to the reduction of the pores with size ranging from ca. 2–6 nm, while the pores larger than 6 nm did not vary to a great extent. The reduction in pore volume at lower pore diameter sizes was more marked in the NiMo/FCNF-450 catalyst, possibly related to a better covering of MoS_2 slabs in this sample.

The total acidity measured by NH_3-TPD in the FCNF-based catalysts (Table 2) showed a drastic reduction compared to the values of the FCNF. Since acidity is attributed to the support itself and not to the metal phase, the lack of acidity can be related to the impossibility of the NH_3 molecules to be adsorbed on the MoS_2 surface. However, the removal of acid sites due to the heat treatment in inert atmosphere during the catalyst preparation cannot be ruled out. No discernible differences between the two carbon-supported catalysts were observed.

Catalysts in the sulfided form were subjected to TPR-S studies. This technique has been used previously for sulfided NiMo catalysts and it provides a measure of chemical reactivity [40]. H_2 consumption is assigned to transition metal species on the surface involved in reactions leading to the formation of a surface anion vacancy, which is subsequently correlated to a catalytic active site [41,42]. Fig. 7 shows the TPR-S profiles, in which a prominent peak centred at ca. 300 °C can be observed for both catalysts, as previously reported for NiMo catalysts supported on active carbon (AC) [43]. The chemical nature of the reactant sulfur in this region can probably be assigned to two different contributions: (i) non-stequiometric sulfur atoms (S_x) weakly adsorbed on coordinated unsaturated edge/corner sites (CUS) [44,45], and (ii) recombination of –SH groups and/or reaction of –SH groups with H_2 [46]. Additionally, a shoulder at temperatures between 350 and 500 °C was observed, assigned to the hydrogenation of S species more labile than stochiometric sulfides, probably consisting of surface anions located at the edges of the crystallites [47]. The reduction of MoS_2-like species in supported catalysts occurs at high temperatures (700–900 °C) [40,45] and could not be determined with these samples due to the carbonaceous nature of the support, which would lead to its hydrogasification.

The amount of H_2 consumed in the low temperature region was much higher for NiMo/FCNF-450 than for NiMo/FCNF-600. This fact is indicative of different amounts of weakly bonded sulfur species on the catalyst surface, implying that the sample tempered at low temperature has a larger number of CUS. This observation is in complete agreement with the XRD and Raman results, which showed that less crystalline MoS_2 species were obtained with the sample treated at low temperature, implying larger amount of defects and vacancies that may act as active sites for hydroprocessing reactions.

3.3. Catalysts performance in heavy oil hydroprocessing

FCNF-supported NiMo catalysts were tested in a batch reactor in the hydroprocessing of a vacuum residue, whose properties are described in Table 1. In order to assess the catalyst performance, asphaltene conversion and $C_{>450\,°C}$, as well as sulfur and metal (Ni and V) removal were determined. In all cases, catalyst performance was benchmarked against a mesoporous alumina-supported NiMo catalyst, $NiMo/Al_2O_3$. The metal content of both catalysts was calculated to have the same metal oxide loading of 3 wt% NiO and 14 wt% MoO_3.

3.3.1. $C_{>450\,°C}$ and asphaltene conversion

The conversions of the fraction boiling above 450 °C ($C_{>450\,°C}$) and asphaltenes ($C_{Asphaltenes}$) are shown in Table 3. Values for $C_{>450\,°C}$ were similar for both FCNF-supported catalysts (ca. 0.50), and slightly lower than that obtained for $NiMo/Al_2O_3$ (0.55). It has been reported that the upgrading of the >450 °C fraction in VR can be mainly considered as a thermally driven process [23,48] thus explaining the small differences observed between catalysts.

A different behaviour was observed in $C_{Asphaltenes}$ for the three catalysts tested. $C_{Asphaltenes}$ was significantly higher for

Table 3
Conversion values for the >450 °C fraction ($C_{>450\,°C}$), asphaltenes ($C_{Asphaltenes}$), HDS and HDM with NiMo/FCNF-T and NiMo/Al_2O_3. All reactions lasted 60 min at 425 °C with an initial 185 bar H_2 pressure. Coke content was determined by TGA. Data of a benchmark catalyst (NiMo/Al_2O_3) are also included for comparison purposes.

Sample	$C_{>450\,°C}$	$C_{Asphaltenes}$	HDS	HDM	C_{Ni}	C_V	Coke ($g_{coke}\ g_{cat}^{-1}$)
NiMo/FCNF-450	0.51	0.73	0.83	0.86	0.67	0.94	0.047
NiMo/FCNF-600	0.49	0.57	0.78	0.74	0.46	0.85	0.081
NiMo/Al_2O_3	0.55	0.59	0.9	0.97	0.95	0.98	0.284

NiMo/FCNF-450 (0.73) compared to NiMo/FCNF-600 (0.57). The Al_2O_3-supported catalyst underperformed NiMo/FCNF-450 in terms of asphaltene conversion and yielded a similar conversion to NiMo/FCNF-600. Therefore, it can be concluded that the decomposition temperature had a strong effect on catalyst performance. This can be attributed to the larger amount of CUS available in the FCNF catalyst subjected to decomposition at low temperature, as deduced from the TPR-S study shown in Fig. 7. This fact can also be the reason for the better performance of the NiMo/FCNF-450 catalyst compared to NiMo/Al_2O_3, since the latter presents a much higher support–metal interaction that may prevent the complete sulfidation of the metal active phase. However, better hydrogen transfer properties of the carbon-based catalyst cannot be ruled out. A metal-free AC was shown to be effective in hydrogen transfer to anthracene [11], which is indicative of the fact that carbon supports may promote monoatomic hydrogen transfer, as stated in [12]. The amount of coke deposited on the catalysts was significantly lower for the FCNF-supported ones (0.047 and 0.081 $g_{coke}\ g_{cat}^{-1}$, compared to 0.284 $g_{coke}\ g_{cat}^{-1}$ for NiMo/Al_2O_3, as observed in Table 3). This can be clearly associated to the higher acidity of Al_2O_3 as a catalyst support (Table 2) and may also help explain the better performance of the FCNF-based catalysts.

There is scarce information about the performance of CNF-supported catalysts on asphaltene upgrading, although ACs have been successfully used as catalytic support in the hydroprocessing of heavy feeds. Moreover, it has been suggested that an AC-supported catalyst limited the condensation reactions of asphaltenes that led to coke formation by providing adsorption sites to the free radicals, thus avoiding polymerisation reactions [49].

3.3.2. Heteroatom removal

HDS and HDM conversions for both NiMo/FCNF and NiMo/Al_2O_3 are presented in Table 3. Ni and V removal data are also included.

The comparison between the two FCNF-supported catalysts in terms of HDS and HDM conversions revealed the same trend observed for VR upgrading in terms of $C_{>450\,°C}$ and $C_{Asphaltenes}$. The catalyst tempered at 450 °C performed better that the one tempered at 600 °C. From the data reported in Table 3, it was observed that the CNF-supported catalysts were more effective in V removal than in Ni removal. However, HDM and HDS conversions obtained with NiMo/Al_2O_3 were higher than the CNF-supported catalysts. It is known that the tendency to form coke is highly related to the HDS and HDM activity [50]. The higher coke deposits obtained with NiMo/Al_2O_3 would allow for the removal of a larger fraction of heteroatoms present in coke precursor molecules in the VR. It is known that coke deposition on hydrotreating catalysts predominantly occurs at early stages of reaction, and it is followed by a steady state in which coke does not affect catalyst stability [51]. In this work, 1 h reaction tests were performed in a batch reactor and the amount of coke deposited can be considered relatively large as a proportion of the feed. Longer reaction times or tests in a continuous flow reactor would be necessary to evaluate the long term activity of the FCNF-supported catalysts.

Similar HDS activities were reported for NiMo supported on conventional alumina and on CNT using a LGO as feedstock [13]. However, CoMo/CNT catalysts tested in the HDS of VR showed slightly lower activities than a CoMo/Al_2O_3 catalyst [21]. No studies on the HDM properties of CNT- or CNF-supported catalysts were found for comparison, although it has been reported that the use of a CoMo catalyst supported on AC led to lower HDM and HDS activity than the corresponding catalyst supported on Al_2O_3 [52]. Overall, good results were obtained in this work when processing a VR with high metal content, compared to the quoted literature which used LGO or a Maya crude with lower heteroatom content.

4. Conclusions

NiMo catalysts supported on functionalised CNF were synthesised. Catalysts were prepared by the direct formation of MoS_2 on the FCNF due to the utilisation of a Mo precursor based on a thiomolybdate complex. The synthesis of fishbone CNF coated with MoS_2 nanosheets decorated with Ni was achieved. The decomposition temperature had a strong effect on the uniformity and homogeneity of the MoS_2 slabs. For the catalyst tempered at 450 °C, long MoS_2 slabs covered the FCNF homogeneously whereas when a tempering temperature of 600 °C was employed, a less homogenous covering of the FCNF was observed. The presence of MoS_2 was confirmed for both catalysts. The number of CUS present in the samples was dependent on the decomposition temperature. This correlated well with the activity of these materials in the hydroprocessing of a VR at 425 °C. The conversion of asphaltenes was higher for the catalyst tempered at 450 °C. This catalyst also outperformed a benchmark NiMo/Al_2O_3 that was used in the same reaction conditions. It is thought that the lower metal–support interaction of the carbon-supported catalyst allowed a more complete sulfidation of the active phase in comparison to NiMo/Al_2O_3. The amount of coke deposited was lower on the carbon-supported catalysts, which may also explain their better performance. On the other hand, higher HDM and HDS conversions were obtained with NiMo/Al_2O_3 than with the CNF-supported catalysts. This can be related to the larger carbon deposits on the former catalyst which would be predominantly formed by asphaltenic structures possibly containing high concentrations of heteroatoms and metals. This study shows that catalysts supported on functionalised CNF have a high potential in heavy feed hydroprocessing.

Acknowledgements

J.L.P. thanks the Spanish MEC for a personal grant (Spanish Scientists Mobility Program, ref. EX2009-0822). H.P., D.T and S.d.LL. thank CSIC for the funding of the short stays at ICB-CSIC or Imperial College (project I-LINK ref. 0439). H.P. and S.d.LL. thank the support of CONACYT Mexico and DGA (Spain), respectively, for the award of their Ph.D. grant. DT thanks the support of FEDER and Spanish Ministery of Economy and Competitiveness for the award of his Ph.D. grant under the frame of the research project ENE2011-28318-C03-01.

References

[1] G.M.K. Abotsi, A.W. Scaroni, Fuel Process. Technol. 22 (1989) 107–133.
[2] F. Rodríguez-reinoso, Carbon 36 (1998) 159–175.
[3] S. Iijima, Nature 354 (1991) 56–58.
[4] Y. Li, D. Li, G. Wang, Catal. Today 162 (2011) 1–48.

[5] J.L. Pinilla, S. De Llobet, I. Suelves, R. Utrilla, M.J. Lázaro, R. Moliner, Fuel 90 (2011) 2245–2253.
[6] S. de Llobet, J.L. Pinilla, M.J. Lázaro, R. Moliner, I. Suelves, Int. J. Hydrogen Energy 37 (2012) 7067–7076.
[7] I. Martin-Gullon, J. Vera, J.A. Conesa, J.L. González, C. Merino, Carbon 44 (2006) 1572–1580.
[8] J. Zhu, A. Holmen, D. Chen, ChemCatChem 5 (2013) 378–401.
[9] J.K. Chinthaginjala, K. Seshan, L. Lefferts, Ind. Eng. Chem. Res. 46 (2007) 3968–3978.
[10] E. Furimsky, Carbons and Carbon Supported Catalysts in Hydroprocessing, Royal Society of Chemistry, Cambridge, UK, 2008.
[11] Z.G. Zhang, T. Yoshida, Energy Fuels 15 (2001) 708–713.
[12] Y.-M. Ma, X.-Y. Wei, X. Zhou, K.-Y. Cai, Y.-L. Peng, R.-L. Xie, Y. Zong, Y.-B. Wei, Z.-M. Zong, Energy Fuels 23 (2009) 638–645.
[13] I. Eswaramoorthi, V. Sundaramurthy, N. Das, A.K. Dalai, J. Adjaye, Appl. Catal., A 339 (2008) 187–195.
[14] K. Dong, X. Ma, H. Zhang, G. Lin, J. Nat. Gas Chem. 15 (2006) 28–37.
[15] Z. Yu, L.E. Fareid, K. Moljord, E.A. Blekkan, J.C. Walmsley, D. Chen, Appl. Catal., B 84 (2008) 482–489.
[16] D. Sebastián, J.C. Calderón, J.A. González-Expósito, E. Pastor, M.V. Martínez-Huerta, I. Suelves, R. Moliner, M.J. Lázaro, Int. J. Hydrogen Energy 35 (2010) 9934–9942.
[17] M.L. Toebes, F.F. Prinsloo, J.H. Bitter, A.J. Van Dillen, K.P. De Jong, J. Catal. 214 (2003) 78–87.
[18] V.R. Surisetty, A. Tavasoli, A.K. Dalai, Appl. Catal., A 365 (2009) 243–251.
[19] G.L. Bezemer, J.H. Bitter, H.P.C.E. Kuipers, H. Oosterbeek, J.E. Holewijn, X. Xu, F. Kapteijn, A.J. Van Diilen, K.P. De Jong, J. Am. Chem. Soc. 128 (2006) 3956–3964.
[20] H. Shang, C. Liu, Y. Xu, J. Qiu, F. Wei, Fuel Process. Technol. 88 (2007) 117–123.
[21] C. Li, B. Shi, M. Cui, H.Y. Shang, G.H. Que, J. Fuel Chem. Technol. 35 (2007) 407–411.
[22] J.L. Pinilla, R. Utrilla, M.J. Lázaro, I. Suelves, R. Moliner, J.M. Palacios, Int. J. Hydrogen Energy 34 (2009) 8016–8022.
[23] H. Purón, J.L. Pinilla, C. Berrueco, J.A. Montoya De La Fuente, M. Millán, Energy Fuels 27 (2013) 3952–3960.
[24] C. Lesaint, W.R. Glomm, Ø. Borg, S. Eri, E. Rytter, G. Øye, Appl. Catal., A 351 (2008) 131–135.
[25] S.F. Zhang, B. Xu, A.A. Herod, R. Kandiyoti, Energy Fuels 10 (1996) 733–742.
[26] M. Millan, C. Adell, C. Hinojosa, A.A. Herod, D. Dugwell, R. Kandiyoti, Energy Fuels 21 (2007) 1370–1378.
[27] P. Serp, M. Corrias, P. Kalck, Appl. Catal., A 253 (2003) 337–358.
[28] J.L. Figueiredo, M.F.R. Pereira, M.M.A. Freitas, J.J.M. Órfão, Carbon 37 (1999) 1379–1389.
[29] K.S.W. Sing, Pure Appl. Chem. 57 (1985) 603–619.
[30] P. Serp, J.L. Figueiredo, Carbon 34 (1996) 1452–1454.
[31] K.P. De Jong, J.W. Geus, Catal. Rev. Sci. Eng. 42 (2000) 481–510.
[32] J.W. Snoeck, G.F. Froment, M. Fowles, J. Catal. 169 (1997) 240–249.
[33] L. Ma, W.-X. Chen, Z.-D. Xu, J.-B. Xia, X. Li, Nanotechnology 17 (2006) 571.
[34] H.J. Liu, Y. Feng, K.W. Ding, S.Y. Huang, G. Qian, Surf. Coat. Technol. 213 (2012) 202–206.
[35] J.L. Brito, M. Ilija, P. Hernández, Thermochim. Acta 256 (1995) 325–338.
[36] G. Alonso, M. Del Valle, J. Cruz, A. Licea-Claverie, V. Petranovskii, S. Fuentes, Catal. Lett. 52 (1998) 55–61.
[37] A. Müller, T. Weber, Appl. Catal. 77 (1991) 243–250.
[38] F.R. Brown, L.E. Makovsky, K.H. Rhee, J. Catal. 50 (1977) 385–389.
[39] B. Windom, W.G. Sawyer, D. Hahn, Tribol. Lett. 42 (2011) 301–310.
[40] B. Scheffer, N.J.J. Dekker, P.J. Mangnus, J.A. Moulijn, J. Catal. 121 (1990) 31–46.
[41] N.K. Nag, D. Fraenkel, J.A. Moulijn, B.C. Gates, J. Catal. 66 (1980) 162–170.
[42] P. Afanasiev, Appl. Catal., A 303 (2006) 110–115.
[43] J. Matos, J.L. Brito, J. Laine, Appl. Catal., A 152 (1997) 27–42.
[44] B. Liu, Y. Chai, Y. Wang, T. Zhang, Y. Liu, C. Liu, Appl. Catal., A 388 (2010) 248–255.
[45] P.J. Mangnus, A. Riezebos, A.D. Vanlangeveld, J.A. Moulijn, J. Catal. 151 (1995) 178–191.
[46] E. Puello-Polo, A. Gutiérrez-Alejandre, G. González, J.L. Brito, Catal. Lett. 135 (2010) 212–218.
[47] C. Calais, N. Matsubayashi, C. Geantet, Y. Yoshimura, H. Shimada, A. Nishijima, M. Lacroix, M. Breysse, J. Catal. 174 (1998) 130–141.
[48] R.M. Gray, Upgrading Petroleum Residues and Heavy Oils, vol. 56, CRC press, 1994.
[49] H. Fukuyama, S. Terai, Pet. Sci. Technol. 25 (2007) 231–240.
[50] M. Absi-Halabi, A. Stanislaus, D.L. Trimm, Appl. Catal. 72 (1991) 193–215.
[51] J.M. Oelderik, S.T. Sie, D. Bode, Appl. Catal. 47 (1989) 1–24.
[52] S.K. Maity, E. Blanco, J. Ancheyta, F. Alonso, H. Fukuyama, Fuel 100 (2012) 17–23.